Green's Function of an Infinite Slot Printed Between Two Homogeneous Dieletrics—Part II: Uniform Asymptotic Solution

Stefano Maci, *Fellow, IEEE,* and Andrea Neto, *Member, IEEE*

***Abstract*—This second part of a two-paper sequence deals with the uniform asymptotic description of the Green's function of an infinite slot printed between two different homogeneous dielectric media. Starting from the magnetic current derived in Part I, the dyadic Green's function is first formulated in integral form in both spectral and spatial domains; next, the asymptotic solution for the vector potential is evaluated asymptotically. The asymptotic ray-field is structured in three contributions: a spherical wave radiated by the source (space wave), a conical leaky wave, and a lateral wave. These contributions are first introduced by the stationary phase method applied to the space-domain radiation integral. From this approach it is seen that the lateral wave contribution is negligible in actual configurations. Next, a rigorous uniform asymptotic evaluation of the radiated field is formulated in the spectral domain by using a steepest descent path deformation which accounts for the vicinity of the pole to the saddle point. Through this rigorous asymptotics, the domain of existence of the leaky-wave is found to be limited by a conical shadow boundary which deviates from that defined by the stationary phase regime. Along this conical shadow boundary, phase matching occurs between space and leaky wave, which facilitates the transition mechanism between the two wave types. This transition occurs inside a conical transition region with elliptical cross section. The interference between space and leaky waves from the near to the far zone are discussed by means of illustrative examples, which also confirm the accuracy of the asymptotics.**

***Index Terms*—Green's function, high-frequency techniques, leaky wave antennas, slot antennas, slot lines.**

I. Introduction

In Part I of this paper [1], the magnetic current excited by an electric dipole on a slot printed between two different homogeneous media is derived in analytical form under the weakly restrictive assumption of small slot width in terms of a wavelength. The final formulation in [1] agrees with the general conclusions discussed in [2] and based on the theory presented in a series of papers [3]–[5] which categorizes the asymptotic currents for a quite general class of guiding structures.

This second part of the paper presents the slot dyadic Green's function and the relevant uniform asymptotic solution valid in any space points. Our formulation is based on the representation of a continuous spectrum of modes which has poles at the solution of the dispersion equation, i.e., at the complex wavenumbers of the leaky-wave guided modes. A general treatment of the continuous spectrum of modes for open ended waveguides can be found in [6], with emphasis on slot lines (see chapters 7 and 8, and reference therein). In particular, the problem of coupling between dipole sources placed in vicinity of a slot line etched on a rectangular waveguides has been treated in [11], and described in terms of asymptotic leaky-wave ray contributions, with similarity and agreement with the description provided here. Another problem which has similar physical contents is that of a semi-infinite transmission line fed by a leaky mode, which is treated in [7].

The paper is structured as follows. In Section II, after a summary of the principal results of Part I [1] relevant to the magnetic currents, the dyadic Green's function is expressed in terms of the electric field potential. In Section III, a stationary phase approximation of the spatial radiation integral of the magnetic currents, provides a ray description in terms of leaky, lateral, and space waves. This physically meaningful representation prepares the rigorous spectral domain asympotics presented in Section IV, which is formulated by a pole-saddle point steepest descent path evaluation of the spectral radiation integral. The final output is a uniform field-potential at any observation aspects, tested and discussed in Section V by means of numerical examples. Conclusions are drawn in Section VI.

II. Dyadic Green's Function

The geometry of the problem is presented in [1, Fig. 1]; it consists of an infinite x-oriented slot which is printed on an infinite ground plane between two homogeneous dielectric half-spaces of permittivities $\epsilon_{r2}(z>0)$, and $\epsilon_{r1}(z<0)$, with $\epsilon_{r2} > \epsilon_{r1}$ assumed for convenience. The cross section w_s of the slot is uniform in x and small in terms of a wavelength. The structure is excited by a y-oriented electric dipole of the same length of the slot width w_s, placed at the origin of the reference system. In addition, ρ_t and r are the distances of the observation point from x and from the origin, respectively, γ is the angle that the observation direction forms with the positive x axis.

A. Magnetic Currents

The closed form expression for the slot magnetic currents derived in [1] was factorized as $m(x,y) = m_t(y)v(x)$, where the

Manuscript received January 25, 2002; revised August 19, 2002. Part of the work of A. Neto was performed at the Jet Propulsion Laboratory, California Institute of Technology under contract with the National Aeronautics and Space Administration. The work of S. Maci was supported by the Italian Space Agency (ASI).

S. Maci is with the Department of Information Engineering, University of Siena, Siena 53100, Italy (e-mail: macis@ing.unisi.it).

A. Neto is Presently with the FEL-TNO, Den Haag, 2597 AK, The Netherlands (e-mail: neto@ing.unisi.it).

Digital Object Identifier 10.1109/TAP.2004.825500

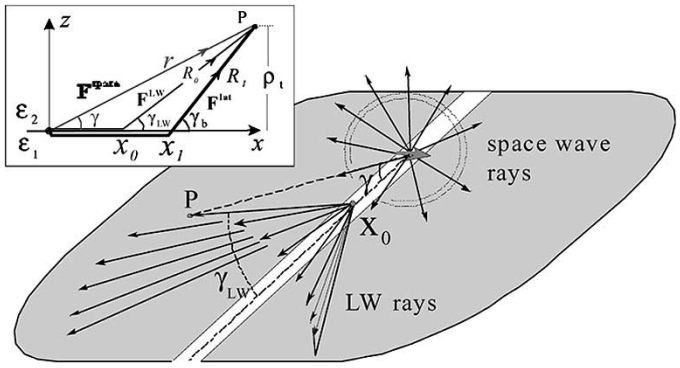

Fig. 1. Ray contributions in the denser medium. Space-wave ray propagate directly from the source with spherical spreading factor. Lateral- and leaky-wave ray arise from x_0 and x_1, respectively, and next propagate toward P with the medium 2 wave speed. Both the leaky wave and the lateral wave have a conical wave-front (only the leaky wave is shown in the three-dimensional (3-D) view) with different spreading factor.

transverse factor $m_t(y)$ is reported in [1, eq. (4)] while the longitudinal factor $v(x)$ has been represented via its Fourier spectrum $1/D(k_x)$ with denominator given by

$$D(k_x) = \frac{1}{2k_0\zeta_0}\sum_{i=1}^{2}(k_i^2 - k_x^2)J_0\left(\frac{w_s}{4}\sqrt{k_i^2 - k_x^2}\right) \times H_0^{(2)}\left(\frac{w_s}{4}\sqrt{k_i^2 - k_x^2}\right) \quad (1)$$

In (1) k_0 and ζ_0 are the free-space propagation constant and the characteristic impedance, respectively; $k_i = k_0\sqrt{\epsilon_{ri}}$ for $i = 1$, 2 are the propagation constants in the two media. In (1), J_0 is the Bessel function of zero order and $H_0^{(2)}$ is the Hankel function of zero order and second kind. Both quasistatic and asymptotic expressions for the spectral representation of $v(x)$ have been given in [1]. The key formulas are

$$v(x) \approx \frac{(k_0\zeta_0\pi w_s)(k_1H_1^{(2)}(k_1|x|) - k_2H_1^{(2)}(k_2|x|))}{4(k_1^2 - k_2^2)|x|} \approx \frac{-jk_0\zeta_0 w_s \ln(x)}{2(k_1^2 - k_2^2)} \quad \text{for } x \text{ small} \quad (2)$$

$$v(x) \sim \frac{\exp(-jk_x^{\mathrm{LW}}|x|)}{jD'(k_x^{\mathrm{LW}})} + v_{10}\frac{e^{-jk_1|x|}}{(k_1x)^2} + v_{20}\frac{e^{-jk_2|x|}}{(k_2x)^2} \quad \text{for } x \text{ large} \quad (3)$$

where $D'(k)$ is the derivative of $D(k_x)$. The coefficients v_{10} and v_{20} are given in [1, eqs. (29) and (30)]. The first term in (3) is a leaky wave that propagates along x with phase constant $\beta_{\mathrm{LW}} = \mathrm{Re}\left(k_x^{\mathrm{LW}}\right)$ and attenuation constant $\delta_{\mathrm{LW}} = \mathrm{Im}\left(k_x^{\mathrm{LW}}\right)$; a well tested approximation for actual slot widths is given in [1, eq. (19)]. From this approximation it is seen that when slot tends to be narrower the propagation constant approaches $\beta = \sqrt{(k_2^2 + k_1^2)/2}$. In any case, the behavior of β_{LW} is weakly dependent on the slot width and on the frequency. The leaky wave phase velocity $\omega/\beta_{\mathrm{LW}}$ is greater than the speed of light in the upper (denser) medium and less than that in the lower medium.

The last two terms at the right-hand side (RHS) of (3), represent *lateral waves* which asymptotically decay as $(x)^{-2}$ and propagate with phase velocity of the upper and lower medium, respectively. Denomination lateral wave has been used here in analogy with the problem of the semi-infinite homogeneous space, where a pair of waves with same phase velocities occur [8]. In [1] it is seen that the lateral wave contributions asymptotically recovers the fringe field $v(x') - v_{\mathrm{LW}}(x')$ for $x > 0.5\lambda_{\mathrm{eq}}$, where λ_{eq} is the equivalent wavelength associated with the average of the permittivities.

B. Vector Potential

The x-oriented electric vector potential, associated with the equivalent magnetic currents defined in (1), will be considered both in the spatial and in the spectral domain. The spatial domain representation in medium $n = 1 (z < 0)$ and $n = 2 (z > 0)$, is

$$F_n(x,y,z) = (-1)^n \int_{-\infty}^{\infty}\int_{-w_s/2}^{w_s/2} \frac{e^{-jk_nR(x-x',y-y',z)}}{4\pi R(x-x',y-y',z)} \times 2m(x',y')dx'dy' \quad (4)$$

where $R(x,y,z) = \sqrt{x^2+y^2+z^2}$ and the factor 2 comes for the application of the image principle (note that for simplicity, we use here a definition of the potential without multiplication for the permittivity). By using the Fourier spectral representation of the scalar, homogeneous-space Green's function, and observing that the Fourier transform of $m(x,y)$ in (1) is $-J_0\left((1/2)w_sk_y\right)/D(k_x)$, we obtain the spectral integral version of (4)

$$F_n(x,y,z) = \frac{(-1)^{(n-1)}}{8\pi^2}\int_{-\infty}^{\infty}\int_{\infty}^{\infty} \frac{J_0(\frac{1}{2}w_sk_y)}{jk_{zn}D(k_x)} \times 2e^{-j(k_xx+k_yy+k_{zn}|z|)}dx'dy' \quad (5)$$

where $k_{zn} = \sqrt{k_n^2 - k_x^2 - k_y^2}$

The remainder of this paper will be concerned with the asymptotic approximation of F_n. This asymptotic treatment provides the basic physical insight for the comprehension of the vector field mechanisms. Analytical derivation of the vector field can be obtained via derivations from the asymptotic potential presented hereinafter.

We will focus the attention on the potential of medium 2, where the leakage occurs. To identify the ray contributions in the asymptotic regime, let us first preliminarily approximate the field potential in (4) and (5) (medium 2) for w_s small with respect to the wavelength, i.e.

$$F_2 \sim -\int_{-\infty}^{\infty}\frac{e^{-jk_2R(x-x')}}{4\pi R(x-x')}2v(x')dx' \quad (6)$$

and

$$F_2 \sim -\frac{1}{4\pi}\int_{-\infty}^{\infty}\frac{H_0^{(2)}\left(\sqrt{k_2^2-k_x^2}\rho_t\right)}{jD(k_x)}e^{-jk_xx}dk_x \quad (7)$$

where $R(x-x') = \sqrt{(x-x')^2+y^2+z^2} = \sqrt{(x-x')^2+\rho_t^2}$. In deriving (6) we have used the approximation $\int_{-w_s/2}^{w_s/2} m_t(y')e^{-jk_xy'}dy' \approx \int_{-w_s/2}^{w_s/2} m_t(y')dy' = -1$, which is valid for w_s small in terms of the wavelength. The same small width approximation applied to the spectral version in (5) imposes $J_0((1/2)w_sk_y) \approx 1$ which, together with the identity

TABLE I
CRITICAL POINT AND ASYMPTOTIC CONTRIBUTIONS IN THE SPACE DOMAIN

Wave type	spatial domain critical points ($x=\rho_t cot\gamma=rcos\gamma$)	kind of critical point
Space wave (F^{space})	$x=0$	log. branch-point
Leaky wave (F^{LW})	$x_o = x - \rho_t cot\gamma_{LW} = \frac{r\,sin(\gamma_{LW}-\gamma)}{sin\gamma_{LW}}$; $\gamma_{LW} = \cos^{-1}\left(\frac{\beta_{LW}}{k_2}\right)$	stationary phase point $\frac{\partial}{\partial x'}(k_2 R(x-x')+\beta_{LW}x)\big\vert_{x'=x_o}=0$
Lateral wave (F^{lat})	$x_1 = x - \rho_t \cot\gamma_b = \frac{r\,sin(\gamma_b-\gamma)}{sin\gamma_b}$; $\gamma_b=\cos^{-1}(k_1/k_2)$	stationary phase point $\frac{\partial}{\partial x'}(k_2 R(x-x')+k_1 x)\big\vert_{x'=x_1}=0$

$\int_{-\infty}^{\infty}(e^{-(k_y y+k_{z2}|z|)}/k_{z2})dk_y = \pi H_0^{(2)}\left(\sqrt{k_2^2-k_x^2}\rho_t\right)$, leads to (7). Note that the *approximate* expressions (6) and (7), are related by an *exact* Fourier transform relationships, as inferred by interpreting the Hankel function in (7) as the Fourier transform of $e^{-jk_2R(x-x')}/R(x-x')$.

III. RAY DESCRIPTION VIA SPATIAL DOMAIN INTEGRATION

The ray description provides a physically appealing picture of the radiation mechanism and a simplified description of the rigorous uniform asymptotics presented in Section IV. The ray-asymptotic approximation will be conducted here directly by using the spatial domain convolution (6) with the scope to clarify the relation between the simple and intuitive spatial-domain critical points from which the ray originate and their spectral counterpart. Insertion of (3) in (6), leads to the following asymptotically dominant critical point in the x' spatial domain.

1) Stationary phase point (SPP) at $x' = x_o$ associated to the leaky wave current contribution in (3); x_0 satisfies the equation $\partial/\partial x'(k_2R(x-x')+\beta_{\rm LW}x)|_{x'=x_o}=0$; the corresponding stationary phase field contribution $F^{\rm LW}$ will be denoted by leaky-wave ray.
2) SPP at $x' = x$ associated to the lateral wave propagating with the wavenumber of medium 1, which satisfies the equation $(\partial/\partial x')(k_2R(x-x')+k_1x)|_{x'=x_1}=0$; The corresponding stationary phase field contribution $F^{\rm lat}$ will be denoted by lateral-wave ray.
3) Log-type branch point singularity at $x'=0$, associated to a field contribution $F^{\rm space}$, denoted by space-wave ray, which is interpreted as the field radiated by the dipole source itself modulated by the presence of the slot.

It is worth emphasizing that no stationary phase points occur for the radiation integral of the lateral-wave that has the intrinsic phase velocity of medium 2. The explicit expressions of the critical points are found in Table I. The above space domain formulation can be summarized as follows:

$$F_2 \sim F^{\rm LW}+F^{\rm lat}+F^{\rm space} \tag{8}$$

$$F^{\rm LW} = \frac{2}{jD'(k_x^{\rm LW})}\int_{\text{“}x_0\text{”}}\frac{e^{-j(k_2R(x-x')+\beta_{\rm LW}x)}}{4\pi R(x-x')}e^{-\delta_{\rm LW}x}dx' \tag{9}$$

$$F^{\rm lat} = 2v_{10}\int_{\text{“}x_1\text{”}}\frac{e^{-j(k_2R(x-x')+k_1x)}}{4\pi\, R(x-x')(k_1x)^2}dx' \tag{10}$$

$$F^{\rm space} = -\int_{\text{“}0\text{”}}\frac{e^{-jk_2R(x-x')}}{4\pi R(x-x')}2v(x')dx' \tag{11}$$

where the subscripts “x_0,” “x_1,” and “0” denote the fact that the integration is performed locally around the corresponding critical point. The RHS of (9) and (10) can be evaluated by the ordinary application of the stationary phase method [8], i.e., by approximating the phase at the second order around the stationary phase point. The space contribution in (11) is instead calculated by linear approximation of the phase around the origine ($k_2R(x-x') \approx k_2r(1-\cos\gamma)$ thus, obtaining $F^{\rm space} \sim (-2e^{-jk_2r}/4\pi r)\int_{-\infty}^{\infty}\exp(jk_2\cos\gamma x')v(x')dx'$, where γ is the angle of the observation point with respect to the slot (see Fig. 1). In this last expression of $F^{\rm space}$ we have extended the local integral to all the real axis as usually done in the derivation of localized space asymptotics. Performing the linear phase approximation, the Fourier transform definition of $v(x')$ is recovered, thus obtaining the closed form expression $1/D(k_2\cos\gamma)$. Eventually, the asymptotic ray approximations of (9)–(11) are

$$F^{\rm LW} \sim \frac{-1}{2D'(k_x^{\rm LW})}\sqrt{\frac{2j}{\pi\rho_t\sqrt{k_2^2-(\beta_{\rm LW})^2}}} \times e^{-jk_2R_0}e^{-j\beta_{\rm LW}|x_0|}e^{-\delta_{\rm LW}|x_0|} \tag{12}$$

$$F^{\rm lat} \sim \frac{-j}{2(k_1x_{s1})^2}v_{10}\sqrt{\frac{2j}{\pi\rho_t\sqrt{k_2^2-k_1^2}}}e^{-jk_2R_1}e^{-jk_1|x_1|} \tag{13}$$

$$F^{\rm space} \sim \frac{-1}{D(k_2\cos\gamma)}\frac{e^{-jk_2r}}{2\pi r} \tag{14}$$

where $R_0=R(x-x_0)$; $R_1=R(x-x_1)$, and $\beta_{\rm LW}$ and $\delta_{\rm LW}$ are the leaky wave propagation and attenuation constants, respectively, as defined in [1, eq.(18)]. The validity of (12) is restricted to $x_o>0$ when $x>0$ and for $x_o<0$ when $x<0$; in (13) it should be $|x_1|>0.5\lambda_{eq}$ in order to ensure sufficient accuracy for the asymptotic evaluation of the integrand, as discussed in Section II-A. The asymptotic description in (12)–(14) is valid only when the critical points are well isolated one respect to the other. A uniform asymptotic description which accounts for collapsing of a pair of critical points will be done in Section IV.

Inspection of the phase factors in (12)–(14) leads to an interpretation of the ray-paths of the various ray contributions. (See Fig. 1 and relevant inset.)

1) The leaky-wave ray propagates along the slot up to the point x_0 with phase constant $\beta_{\rm LW}$ and attenuation constant $\delta_{\rm LW}$, and next leaves the slot toward the observer at P, propagating with the ambient wavespeed. All the rays which start from x_0 propagate along the surface of a slot centered radiation cone with angle $\gamma_{\rm LW}=\cos^{-1}(\beta_{\rm LW}/k_2)$ [see Fig. 2(b)].

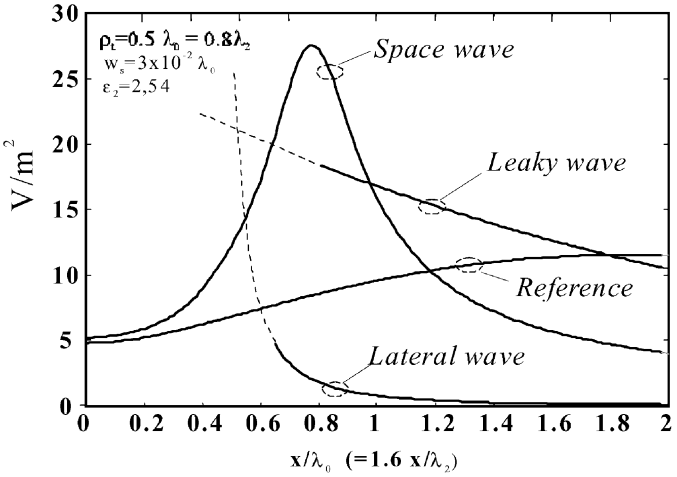

Fig. 2. Ray contributions at a distance 0.5 λ_0 from the slot versus x/λ_0.

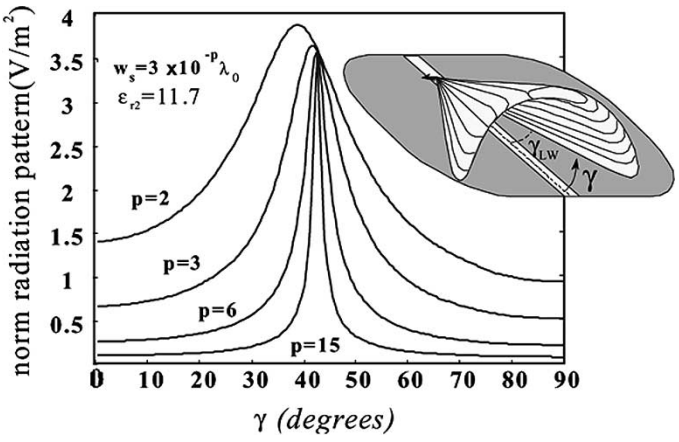

Fig. 3. Electric potential F_2 as a function of γ in the far region, normalized by multiplication for r. Results have been obtained by retaining the space wave contribution (14) alone. Different curves correspond to different slot widths W_s. The denser medium has $\varepsilon_{r2} = 11.7$ (silicon) in contrast with free space ($\varepsilon_{r1} = 1$). The inset shows the conical 3-D radiation pattern with maximum at $\gamma_{\rm LW}$ with respect to the slot axis (only one side is depicted, the pattern has to be duplicated for negative x).

2) The lateral wave contribution propagates along the slot with phase velocity of the lower medium up to x_1, and next reaches P along the ray-path R_1. As for the leaky wave, the lateral wavefront is cylindrical, and the rays emanated from x_1 reach the observer along the surface of a cone with angle $\gamma_b = \cos^{-1}(k_1/k_2)$ Propagating along the slot, the lateral wave exhibits an attenuation inversely proportional to x_1^2.
3) The space-wave rays have a spherical wavefront centered at the dipole source.

A. Asymptotic Orders With Respect to Distance From the Source

It is instructive to reexpress the previous terms in the spherical coordinate system. To this end, we use the identities $x_1 = r\sin(\gamma_b - \gamma)/\sin\gamma_b$ and $x_0 = r\sin(\gamma_{\rm LW} - \gamma)/\sin\gamma_{\rm LW}$ which, for observation in the region $\{x > 0, z > 0\}$, lead to

$$F^{\rm LW} = \frac{-e^{-\delta_{\rm LW} r\sin(\gamma_{\rm LW}-\gamma)/\sin\gamma_{\rm LW}}}{2D'(k_x^{\rm LW})\sqrt{\pi\sin\gamma\sin\gamma_{\rm LW}}} \times \frac{\sqrt{2j}e^{-jk_2 r\cos(\gamma-\gamma_{\rm LW})}}{\sqrt{k_2 r}} \quad \gamma < \gamma_{\rm LW} \tag{15}$$

$$F^{\rm lat} = \frac{-j\sin^2\gamma_b v_{10}}{2\sin^2(\gamma_b-\gamma)\sqrt{\pi\sin\gamma\sin\gamma_b}} \times \frac{\sqrt{2j}e^{-jk_2 r\cos(\gamma-\gamma_b)}}{(k_1 r)^2\sqrt{k_2 r}} \quad \gamma \ll \gamma_b \tag{16}$$

and to a symmetrical solution for $\{x < 0, z > 0\}$. The restriction $\gamma < \gamma_{\rm LW}$ arises from the condition $x_o > 0$ that was applied to (12); $\gamma \ll \gamma_b$ roughly means $x_1 > \lambda_{eq}$ (this condition is not well specified here, details will be given in the next). Equations (15) and (16) exhibit explicitly the asymptotic order with respect to r. The lateral wave decays with order $(k_1 r)^{-2}(k_2 r)^{-(1/2)}$, so it is of higher asymptotic order with respect to leaky-wave $\left((k_2 r)^{-(1/2)}\right)$ and to space-wave $\left((k_2 r)^{-1}\right)$. In order to quantify the relative weight of the various contributions, Fig. 2 presents the potential F_2 at a fixed distance from the slot ($z = 0.50\lambda_0$, $y = 0$) as a function of x/λ_0. The slot width is $w_s = 3\,10^{-2}\lambda_0$, while the two dielectric constants are $\epsilon_{r2} = 2.54$ and $\epsilon_{r1} = 1$. The amplitudes of the leaky, lateral and space waves in (12) and (14) are presented together with a reference plot of the total potential, that is obtained by the numerical space domain integration of (6).

Both leaky- and lateral-wave curves are presented in dashed line for small values of x, because their expressions there lose validity due to the inapplicability of the asymptotic derivation. It is apparent that for observation points close to the source the space-wave almost recovers the total field (reference); for increasing x the LW wave contribution gradually prevails. The lateral wave is almost negligible with respect to the other contributions, due to the higher order asymptotic decay. This also suggests to ignore its contribution in the uniform asymptotic solution given in Section IV.

B. Far-Field Pattern

When observing very far from the source (i.e., in the far field antenna region), the dominating term is the space wave contribution; indeed, in the far-field regime, there exists a direct relationship between radiation pattern and current spectrum. The slot antenna exhibits a conical radiation pattern (see inset of Fig. 3) with maximum $\gamma = \gamma_{\rm LW} = \cos^{-1}\left(Re\left(k_x^{\rm LW}\right)/k_2\right)$. This is intuitively justified by the fact that every field contributions from the leaky-wave phased incremental magnetic current superimpose coherently in that direction. Within the ray description of the leaky-wave given above, the angle $\gamma_{\rm LW}$ is also the direction of the leaky-wave rays. This may give the impression that the total far field is produced by the leaky-wave ray alone, which is erroneous; indeed the far field must decay as r^{-1}, while the leaky wave field is of order $r^{-1/2}$.

This apparent puzzling will be clarified successively when the rigorous uniform asymptotics will be derived. Let us just anticipate that in the framework of the asymptotic pole-(saddle-point) description that follows, the leaky wave contribution from the pole residue exists in a region where the leaky wave exhibits exponential attenuation for increasing r, thus rigorously vanishing in the far zone. The far field directive pattern is not then given by the leaky wave ray, but more properly by the enhancement of

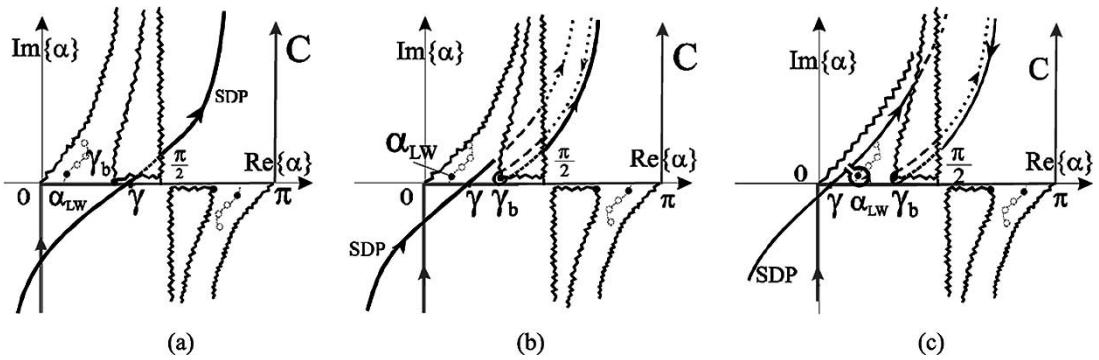

Fig. 4. Angular spectral plane. The original contour $C = (-j\infty, 0, \pi, \pi + j\infty)$ is deformed into the SDP through the saddle point γ. Branch points (b and c) and leaky wave pole (c) are captured in the contour deformation. L-type branch point at γ_b maps the square-root branch cuts at k_1 in the k_x-plane ([1, Fig. 4]). Other log-type branch cuts at γ_b and 0 occur, that correspond to the log-type branch cuts at k_1 and k in the k_x-plane, respectively. The continuous line paths are on the top Rieman sheet (RS) associated with every branch cuts. The long dashed line paths are on top RS of the square-root type branch cut at γ_b and on bottom RS of the log-type branch cut at γ_b. Short dashed line paths are on bottom RS of the square-root type branch cut at γ_b and on top RS of the log-type branch cut at γ_b. Dotted line are on bottom RS of both type of branch cuts at γ_b.

the spectrum $1/D(k_x)$ in (7) which is produced by the vicinity of a leaky-wave pole to the visible region of the k_x spectrum.

Fig. 3 shows the far field radiation pattern, normalized to the observation distance $F_2^{\text{norm}} = F_2 \cdot r$, as a function of the angle γ, for different slot widths ($w_s = 3\,10^{-2}\lambda_0$, $w_s = 3\,10^{-3}\lambda_0$, $w_s = 3\,10^{-6}\lambda_0$, $w_s = 3\,10^{-15}\lambda_0$). The two different dielectrics are air ($\epsilon_{r1} = 1$) and silicon ($\epsilon_{r2} = 11.7$), respectively. Only the scan $\gamma \in (0, 90^\circ)$ is presented since the radiation pattern is symmetric for $\gamma \in (90^\circ, 180^\circ)$.

As the width of the slot decreases, the leaky antenna becomes more directive, since the effective radiating length of the slot increases, as implied by the decreasing of the attenuation constant. As the slot tends to be narrower the propagation constant approaches the value $\beta = \sqrt{(k_2^2 + k_1^2)/2}$, so that $\gamma_{\text{LW}} \to \cos^{-1}\left(\sqrt{(\epsilon_{r1}/\epsilon_{r2} + 1)/2}\right)$.

C. Vector Potential in Medium 1

As far as medium 1 is concerned, the radiation integral does not exhibit any stationary phase contribution, so that the unique contribution is that from the origin. The vector potential can than be very simply evaluated asymptotically by just retaining the space wave contribution; i.e., $F_1 \sim F_1^{\text{space}} = e^{-jk_1 r}/(2\pi r D(k_1 \cos\gamma))$ which is obtained from (14) by replacing k_2 with k_1. This approximation is asymptotically valid starting from a distance comparable with a wavelength of medium 1. Note that this pattern is not directive being the magnetic currents phase velocity of any wave type less than the ambient wavespeed. This also implies that the visible spectral region relevant to medium 1 (i.e., $k_x \in (-k_1, k_1)$) is not affected by the vicinity of the leaky wave pole.

IV. Uniform Asymptotic Solution

The spectral k_x plane for the integrand in (7) is the same as that in [1, Fig. 4], which was associated to the currents, except for an additional saddle point at $k_x = k_s = k_2 \cos\gamma$ introduced by the multiplying factor $\exp(-j\rho_t\sqrt{k_2^2 - k_x^2})$ which is asymptotically introduced by the Hankel function $H_0^{(2)}(\rho_t\sqrt{k_2^2 - k_x^2})$ for large ρ_t . Two branch points are associated to the square roots of the integrand at $k_x = \pm k_1$, $k_x = \pm k_2$, with branch cuts defined such $Im(\sqrt{k_i^2 - k_x^2}) < 0$ on the top Rieman sheet associated to $k_x = \pm k_i$ Logarithmic-type branch points at $k_x = \pm k_i$ $(i = 1, 2)$ are introduced by the annulment of the argument of the Hankel functions in $D(k_x)$, and possess vertical branch cuts. The log-branch cut associated to $k_x = k_1$ is defined on the bottom Rieman sheet of the square root $\sqrt{k_2^2 - k_x^2}$. A "leaky-wave (LW) pole" K_x^{LW}, is located on the top Rieman sheet associated with $\sqrt{k_2^2 - k_x^2}$ (i.e., $Im\sqrt{k_1^2 - (k_x^{\text{LW}})^2} < 0$) and on bottom Rieman sheet associated with $\sqrt{k_2^2 - k_x^2}$ (i.e., $Im\sqrt{k_2^2 - (k_x^{\text{LW}})^2} > 0$). Other poles are located on various combinations of square root Rieman sheets, as discussed in [1]. These further poles don't have any physical meaning because are not captured by any convergent contour deformation. Furthermore, they are far from the real top-sheet axis and therefore their influence on spectral integration is weak. The phase of the three ray contributions discussed in the previous sections arises from the local phase of the integrand at the three critical spectral points, with the following association:

$$\text{Phase of the integrand at } k_x = \beta_{\text{LW}} = Re\left(k_x^{\text{LW}}\right) \to \text{ Phase of the leaky}-\text{wave ray} \quad (17)$$

$$\text{Phase of the integrand at the branch point } K_x = K_1 \to \text{Phase fo the lateral}-\text{wave ray} \quad (18)$$

$$\text{Phase of the integrand at } k_x = k_s \to \text{ phase of the space wave.} \quad (19)$$

A. Angular Spectrum

Introducing the asymptotic approximation of the Hankel function for large argument, and using the change of variable $k_x = k_2 \cos\alpha$ with $\sqrt{k_2^2 - k_x^2} = k_2 \sin\alpha$, the integral in (7) becomes

$$F_2 \sim \int_c e^{-jk_2 r\,\cos(\alpha - \gamma)} f(\alpha) d\alpha$$

$$f(\alpha) = \frac{-\sqrt{2j}\sqrt{k_2 \sin\alpha}}{4\pi j D(k_2 \cos\alpha)\sqrt{r\pi \sin\gamma}} \quad (20)$$

where γ is the angle that the observation vector forms with the positive x axis and C is the contour $(-j\infty, 0, \pi, \pi+j\infty)$ which maps into the angular spectral domain the real axis of the k_x plane. The spectral angular plane is depicted in Fig. 4. The phase of the integrand exhibits a saddle point at $\alpha = \gamma$ which corresponds to the saddle point k_s in the rectilinear spectrum; furthermore, a branch point at $\gamma_b = \cos^{-1}(k_1/k_2)$ and a pole at $\alpha_{\rm LW} = \cos^{-1}(k_x^{\rm LW}/k_2)$ occur, which map the branch point k_1 and the pole $k_x^{\rm LW}$ of the k_x-spectrum, respectively. The branch point due to the square root at k_2 in the rectilinear spectral plane (mapped at points 0 and π in the angular plane) disappeared owing to the angular transformation used which automatically solves the ambiguity of $\sqrt{k_2^2 - k_x^2}$ defining it as $k_2 \sin\alpha$. Note that the log-type singularities at 0 and π still remains; these latter are not however involved in the following asymptotic treatment, as well as the other nonphysical poles.

To perform the asymptotic evaluation of the integral on the original contour C, we deform this contour onto the steepest descent path (SDP) through the saddle point $\alpha = \gamma$. The SDP equation in the plane is defined by $Re(\cos(\alpha - \gamma)) = 1$ with $Im(\cos(\alpha - \gamma)) < 0$. In this deformation either the leaky wave pole $\alpha_{\rm LW}$ or the log-type branch cut at γ_b may be captured depending on the position of the observer. Three different situations may be defined, which are represented in Fig. 4(a)–(c), respectively. When $\gamma > \gamma_b$, [see Fig. 4(a)] neither $\alpha_{\rm LW}$ nor γ_b are captured during the contour deformation; in this case the total field is reconstructed by the sole SDP integration. For $\gamma < \gamma_b$ [see Fig. 4(b)] the branch point γ_b is captured, thus requiring an additional integration around the branch-cut. For $\gamma < \gamma_{sb}$ [see Fig. 4(c)] the pole $\alpha_{\rm LW}$ is captured in the contour deformation, thus leading a residue contribution in addition to the SDP and to the branch cut integrations.

The boundary between the situation of Fig. 4(b) and (c) occurs when the SDP crosses the pole, that is when

$$Re(\cos(\alpha_{\rm LW} - \gamma_{sb})) = 1 \tag{21}$$

which, defining $\alpha_{\rm LW}^{\rm re} = Re(\alpha_{\rm LW})$ and $\alpha_{\rm LW}^{\rm im} = Im(\alpha_{\rm LW})$, implies

$$\gamma = \gamma_{sb} = \alpha_{\rm LW}^{\rm re} + cos^{-1}\left(\frac{1}{\cosh(\alpha_{\rm LW}^{\rm im})}\right). \tag{22}$$

Eventually, the potential F_2 can be expressed as

$$F_2 = I_{\rm sdp} + I_{\rm LW} U(\gamma_{sb} - \gamma) + I_{lat} U(\alpha_b - \gamma) \tag{23}$$

where $U(x)$ is the unit step function ($U(x) = 1$ for $x > 0, U(x) = 0$ for $x < 0$) which accounts for the existence domain of the various contributions as described in Fig. 4(a)–(c). In accordance with the nonuniform ray description in Section III, and on the basis of the phase term inspection in (17)–(19), the mathematical definition and the corresponding physical meaning of the various contributions is as follows:

1) $I_{\rm sdp}$ = SDP integral $\rightarrow$ space wave contribution ($\rightarrow F^{\rm space}$);
2) I_{lat} = integral around the log-branch cut at $\alpha_b \rightarrow$ lateral wave contribution ($\rightarrow F^{\rm lat}$);
3) $I_{\rm LW}$ = residue at $\alpha_{\rm LW} \rightarrow$ leaky wave contribution ($\rightarrow F_{\rm LW}$).

In (23), the unit step functions $U(\gamma_{sb} - \gamma)$ identifies the existence region of the leaky wave inside a shadow boundary cone $\gamma = \gamma_{sb}$. The existence function $U(\gamma_b - \gamma)$ defines a shadow boundary cone (SBC) at $\gamma = \gamma_b$ which bounds the existence region of the lateral wave. The various contribution will be described next.

B. Lateral Wave Contribution

As far as I_{lat} is concerned, its contribution exists for $\gamma < \gamma_b$. We remind that from what found in Section III-B, the lateral wave contribution behaves asymptotically as $(k_1 r)^{-2}(k_2 r)^{-(1/2)}$. In the transition regime ($\gamma \approx \gamma_b$) this contribution must change its spreading factor in $(k_1 r)^{-1}$ to match the space-wave (SDP) contribution. Due to this strong transition of asymptotic order, this contribution is extremely concentrated around the shadow boundary cone $\gamma = \gamma_b$ with very narrow transition region. Actually, in all the practical configurations we have investigated, it has systematically been found negligible due to prevalence of the space-wave contribution. Thus, the corresponding uniform asymptotics will not be presented in this paper to avoid useless mathematical complications. A complete uniform treatment of this contribution fits a general canonical asymptotic scheme, which will be topic of a further work.

C. Leaky-Wave Contribution and Limit to the Ray Description

In (31), the leaky-wave contribution is obtained from the residue of $f(\alpha)$ in (20) as

$$I_{\rm LW} = \frac{-\sqrt{2j}}{2\sqrt{r\pi \sin\gamma}} \frac{e^{-jk_2 r\cos(\alpha_{\rm LW} - \gamma)}}{\sqrt{k_2 \sin\alpha_{\rm LW}}\, D'(k_x^{\rm LW})} \tag{24}$$

or giving explicit evidence to the real part $\alpha_{\rm LW}^{\rm re}$ and the imaginary part $\alpha_{\rm LW}^{\rm im}$ of the complex pole $\alpha_{\rm LW}$, as shown in (25) at the bottom of the page. It is evident that (25) is an evanescent cylindrical wave which propagates with a phase velocity $\omega/(k_2 \cosh(\alpha_{\rm LW}^{\rm im}))$ less than the wavespeed of the ambient medium, and along a direction which forms an angle $\alpha_{\rm LW}^{\rm re}$ with respect to the x axis. Fig. 5 shows a graphical representation of the leaky wave, observed along radial scans from the source, at different γ. The values of the leaky field are proportional to exponentially damped or amplified sinusoids with period $2\pi/(k_2 \cosh(\alpha_{\rm LW}^{\rm im}) \cos(\alpha_{\rm LW}^{\rm re}) \cos(\alpha_{\rm LW}^{\rm re} - \gamma))$ and exponential attenuation $k_2 r \sinh(\alpha_{\rm LW}^{\rm im}) \sin(\alpha_{\rm LW}^{\rm re} - \gamma)$. Along $\gamma = \alpha_{\rm LW}^{\rm re}$ the field is constant along r, being $\alpha_{\rm LW}^{\rm re}$ the angle of LW direction of propagation. Along $\gamma = \alpha_{\rm LW}^{\rm re}$, the

$$I_{\rm LW} = -\sqrt{2j} \frac{e^{-k_2 r \sinh(\alpha_{\rm LW}^{\rm im}) \sin(\alpha_{\rm LW}^{\rm re} - \gamma)} e^{-jk_2 r \cosh(\alpha_{\rm LW}^{\rm im}) \cos(\alpha_{\rm LW}^{\rm re} - \gamma)}}{2\sqrt{r\pi \sin\gamma}\sqrt{k_2 \sin\alpha_{\rm LW}}\, D'(k_x^{\rm LW})} \tag{25}$$

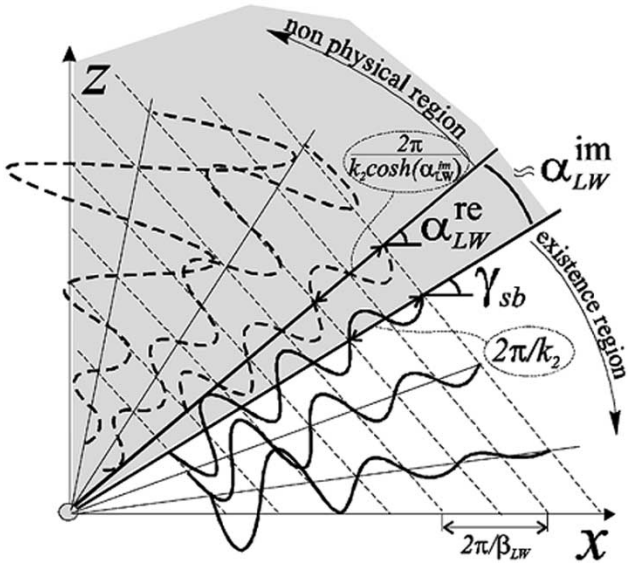

Fig. 5. Graphical representations of the leaky wave along radial scans. Only the case $\gamma < \pi/2$ is depicted, the remaining region being obtainable by symmetry. The leaky-wave is represented as exponentially damped or amplified sinusoids along radial lines according to (25). Dashed straight lines denote the phase (conical) wave-fronts. The LW existence region (defined by pole capturing in the SDP deformation) is for $\gamma < \gamma_{SB}; \gamma > \alpha_{\rm LW}^{\rm re}$ is the unphysical region in which the leaky wave amplify for increasing r. In the existence region, the wave-front velocity along radial lines is always larger than the speed of light in the medium. At $\gamma = \gamma_{SB}$ the radial leaky wave-speed matches the ambient speed of light.

wavelength is $2\pi/\cosh(\alpha_{\rm LW}^{\rm im})$, i.e., shorter than that of the ambient medium (slow wave). For $\gamma > \alpha_{\rm LW}^{\rm re}$ the wave exhibits amplification, so that this region is unphysical. The shadow boundary γ_{sb} occurs for $\gamma_{sb} < \alpha_{\rm LW}^{\rm re}$; consequently in all the region where the LW exists, (i.e., where the pole is captured during the SDP deformation), the LW field exhibits attenuation along the radial scan, as expected. We also note that in the range $\alpha_{\rm LW}^{\rm re} < \gamma < \gamma_{sb}$ the leaky wave is still physical, but it does not exist in the present asymptotic description. Actually, the shadow boundary γ_{sb}, defined mathematically from the interception of the pole with the SDP (21), corresponds through (22) to $\cosh\left(\alpha_{\rm LW}^{\rm im}\right)\cos\left(\alpha_{\rm LW}^{\rm re} - \gamma_{sb}\right) = 1$, i.e., to that radial direction along which the local wavelength is exactly $2\pi/k_2$, namely that of the medium. Thus that *the phase of the leaky-wave matches at γ_{sb} the phase $\exp(-jk_2 r)$ of the space wave* . We will return on this concept in Section IV-E

Let us now consider the dependence of the LW parameter $\alpha_{\rm LW}^{\rm re}$, $\alpha_{\rm LW}^{\rm im}$, γ_{sb} from $\gamma_{\rm LW}$ and $\delta_{\rm LW}$. In Table II, exact mathematical expressions are reported together with the approximation obtained for small values of the leaky attenuation constant $\delta_{\rm LW}(\delta_{\rm LW}/k_2 \ll 1)$. The exact expressions as well as the approximations can be obtained by straightforward algebraic manipulations from the definition of the various parameters. We note that the angle of propagation $\alpha_{\rm LW}^{\rm re}$ is approximated by $\gamma_{\rm LW}$ up to the second order of $(\delta_{\rm LW}/k_2)$ (we remind that $\gamma_{\rm LW}$ identifies the direction of the leaky-wave ray contribution in the stationary phase regime, see Fig. 1). Typical values of the deviation between $\alpha_{\rm LW}^{\rm re}$ and $\gamma_{\rm LW}$ are in the order of one degree. It is also seen that the deviation between the shadow boundary angle γ_{sb} and the direction $\alpha_{\rm LW}^{\rm re}$ of the LW propagation is of order $\delta_{\rm LW}/k_2$ and coincides with $\alpha_{\rm LW}^{\rm im}$ (typical values are about ten degrees). Insertion of the approximation for $\alpha_{\rm LW}^{\rm re}$ and $\alpha_{\rm LW}^{\rm im}$ in (25) recovers the ray contribution $F^{\rm LW}$ in (15) up to the order $\delta_{\rm LW}/k_2$:

$$\lim_{\delta_{\rm LW}/k_2 \to 0} I_{\rm LW} = F^{\rm LW} \tag{26}$$

The small discrepancy between the SDP (spectral) and the stationary phase (spatial) approaches is justified by the fact that the more rigorous SDP approach preserves the exact complex phase of the integrand. The spatial stationary phase result can recover the SDP result when one incorporates in the integrand in (9) the attenuation constant in the total complex phase; thus, the point which annuls the derivative of the space domain phase (i.e., x_0 in Table I) becomes complex and the exact value of the LW residue is reconstructed. However, we should emphasize that the concept of "ray" applied to the leaky wave contribution implies a wavespeed of the ambient medium, and therefore it can be used only in the limit (26).

D. Space-Wave Contribution

The last step in the uniform asymptotic evaluation is the analytical approximation of the integral along the SDP. To this end, we first introduce a change of variable $\cos(\alpha - \gamma) = 1 - js^2$, thus leading to

$$\begin{aligned} I_{\rm sdp} &= \int_{\rm sdp} f(\alpha) e^{-jk_2 r\cos(\alpha-\gamma)} d\alpha \\ &= e^{-jk_2 r} \int_{-\infty}^{\infty} e^{-k_2 r s^2} G(s) ds \end{aligned} \tag{27}$$

where $G(s) = f(\alpha)(d\alpha/ds) = f(\alpha)/\left((1\sqrt{j2})\cos((1/2)(\alpha-\gamma))\right)$. In the s-plane, the saddle point is mapped on $s = 0$, the SDP in the real axis and the leaky wave pole into

$$s_{\rm LW} = \exp\left(-j\frac{\pi}{4}\right)\sqrt{2}\sin\left(\frac{1}{2}(\alpha_{\rm LW} - \gamma)\right). \tag{28}$$

The asymptotic evaluation is performed via the Van der Waerden (VdW) method [9]. The asymptotics is dominated by the saddle point contribution but is sensitive to whether the pole is near the SDP and/or is crossed by the SDP. If the pole and the SDP are distinct, each can be evaluated separately from the other and the ray regime (Section III) is recovered. When the SDP and pole are contiguous, the asymptotics must be refined, i.e., made uniform, to account simultaneously for both; this is the transition region near and across the leaky wave shadow boundary γ_{sb} in physical space. The VdW method proceeds by mapping the given spectral integral onto a canonical integral, which expresses the pole-SDP interaction in the simplest possible manner, in addition to a regular pole-less remainder integral. While there are various asymptotic techniques which yield the decomposition into the transition function plus a regular remainder, we regard the VdW method as the "cleanest" for asymptotic book keeping and best suited for our purposes. Via the VdW method, the pole is extracted from the spectral integrand

$$G(s) = G(s) - \frac{R'}{s - s_{\rm LW}} + \frac{R'}{s - s_{\rm LW}} \tag{29}$$

TABLE II
EXACT AND APPROXIMATE RELATION BETWEEN LW PARAMETERS

parameter	exact expression	approximation for $\frac{\delta_{LW}}{k_2}<<1$
γ_{LW}	$\cos^{-1}\left(\frac{\beta_{LW}}{k_2}\right)$	
$\alpha_{\rm LW}^{re}$	$\alpha_{LW}^{re}=\cos^{-1}\left(\cos\gamma_{LW}\sqrt{1-\left(\frac{\delta_{LW}}{k_2 sin\gamma_{LW}}\right)^2}\right)$	$\gamma_{LW}+\frac{1}{2}\frac{cos(\gamma_{LW})}{sin^2(\gamma_{LW})}\left(\frac{\delta_{LW}}{k_2}\right)^2$
$\alpha_{\rm LW}^{im}$	$\alpha_{LW}^{im}=\frac{1}{2}\,ln\left(\frac{1+\frac{\delta_{LW}}{k_2 sin\gamma_{LW}}}{1-\frac{\delta_{LW}}{k_2 sin\gamma_{LW}}}\right)$	$\frac{1}{sin\gamma_{LW}}\left(\frac{\delta_{LW}}{k_2}\right)$
γ_{sb}	$\alpha_{\rm LW}^{re}+\cos^{-1}\left(\sqrt{1-\frac{(\delta_{LW})^2}{k_2^2 sin^2\gamma_{LW}}}\right)$	$\gamma_{LW}-\frac{1}{sin(\gamma_{LW})}\left(\frac{\delta_{LW}}{k_2}\right)\approx\alpha_{\rm LW}^{re}-\alpha_{\rm LW}^{im}$

thereby isolating the pole contribution from the resulting regularizing remainder $T(s)=G(s)-R'/(s-s_{\rm LW})$, with residue $R'=-\sqrt{2j}/(\sqrt{k_2\sin\alpha_{\rm LW}}D'(k_x^{\rm LW})\sqrt{r\pi\sin\gamma}4\pi j)$.

The asymptotic evaluation proceeds by expanding $T(s)$ in a Taylor series around the saddle point $s=0$, retaining only the first term in the expansion and integrating term by term

$$I_{\rm sdp}\sim\left(G(0)-\frac{R'}{-s_{\rm LW}}\right)\int_{-\infty}^{\infty}e^{-k_2 rs^2}ds + R'e^{-jk_2 r}\int_{-\infty}^{\infty}\frac{e^{-k_2 rs^2}}{s-s_{\rm LW}}ds. \quad (30)$$

After recognizing the canonical integrals in (30) in terms of the Fresnel transition function, we obtain the two alternative expressions shown in (31) and (32) at the bottom of the page, where the upper (lower) sign in (32) applies to $\gamma>\gamma_{sb}$ ($\gamma<\gamma_{sb}$),

$$\operatorname{erfc}(\eta)=\frac{2}{\sqrt{\pi}}\int_{\eta}^{\infty}e^{-t^2}dt \quad (33)$$

and

$$F(\xi)=2j\sqrt{\xi}e^{j\xi}\int_{\sqrt{\xi}}^{\infty}e^{-jt^2}dt;\quad -\frac{3\pi}{2}<arg(y)\le\frac{\pi}{2} \quad (34)$$

is the complex argument analytical continuation of the transition function of the uniform theory of diffraction (UTD) [10]. We note that $F(\xi)\to 1$ for "large" value of its argument ξ, and $\operatorname{erfc}(\eta)\to 1$ for "small" value of its argument η. "Small" and "large" are defined on the basis of the belonging of the observation point to a certain "transition region" defined next. The analytical details for the derivation of (31) and (32), not presented here, can be deduced by those relevant to other diffraction problems like that of a diffraction by an inhomogeneous plane wave at an half-plane edge [11].

E. Asymptotic Synthesis and Uniform Compensation Process

Eventually, the uniform asymptotic field potential in the two media has been found by

$$F_2\sim\tilde{I}_{\rm sdp}+I_{\rm LW}U(\gamma_{sb}-\gamma) \quad (35)$$

for medium 2, while maintaining the simple structure $F_1\sim -e^{-jk_1 r}/(2\pi rD(k_1\cos\gamma))$ (Section III-C) for medium 1. In (35), $I_{\rm LW}$ is given in (25), γ_{sb} in (22), and $\tilde{I}_{\rm sdp}$ in one of the two alternative expressions (31) or (32), which are identical because of the exact mathematical relationship there exists between $\operatorname{erfc}(\eta)$ and $F(\xi)$. The uniform dyadic field can be obtained from (35) by straightforward differentiation.

Inside a certain transition region, the space-wave $\tilde{I}_{\rm sdp}$ modifies its wave structure from spherical to conical in order to compensate for the discontinuity of the leaky wave at the shadow boundary cone.

Accordingly to [11], the transition region can be defined where the error of the erfc function with respect to unity is smaller than an arbitrarily small number ϵ'. To find the shape of the transition region, we thus assume that for a certain small ϵ, $|\operatorname{erfc}(\epsilon)-1|\approx\epsilon'$ unless of terms of order $(\epsilon')^2$. Using the expansion of the erfc, we found $\epsilon'=2\epsilon/\sqrt{\pi}$. It is seen that the transition regions occupy the interior of a conical region with elliptical cross section, as depicted in Fig. 6. The cross-section ellipse, shown in the two-dimensional (2-D) view of Fig. 7, has major axis along the direction $\gamma=\alpha_{\rm LW}^{\rm re}$, one focus at the origine, and the other focus at distance $(\lambda_2/4)(\epsilon'/\alpha_{\rm LW}^{\rm im})^2$. Note that the shadow boundary is tilted with respect to the ellipse orientation and intersects the ellipse at the level of its minimum waist.

Both (31) and (32) are useful for the physical interpretation. For large argument (out from the transition region), (31) is more explicit; indeed, being $F(\xi)\to 1$, the second term at the rhs of

$$I_{\rm sdp}\sim\tilde{I}_{\rm sdp}=-\frac{e^{-jk_2 r}}{2\pi r}\left(\frac{1}{D(k_2\cos\gamma)}+\frac{\left(1-F[2k_2 r\sin^2\left(\frac{1}{2}(\alpha_{\rm LW}-\gamma)\right)]\right)}{2k_2\sin\left(\frac{1}{2}(\alpha_{\rm LW}-\gamma)\right)\sqrt{\sin\gamma\sin\alpha_{\rm LW}}D'\left(k_x^{\rm LW}\right)}\right) \quad (31)$$

$$I_{\rm sdp}\sim\tilde{I}_{\rm sdp}=-\frac{e^{-jk_2 r}}{2\pi r}\left(\frac{1}{D(k_2\cos\gamma)}+\frac{1}{2k_2\sin\left(\frac{1}{2}(\alpha_{\rm LW}-\gamma)\right)\sqrt{\sin\gamma\sin\alpha_{\rm LW}}D'\left(k_x^{\rm LW}\right)}\right) \pm\frac{1}{2}I_{\rm LW}\operatorname{erfc}\left(\mp\sqrt{j2k_2 r}\sin\left(\frac{1}{2}(\alpha_{\rm LW}-\gamma)\right)\right) \quad (32)$$

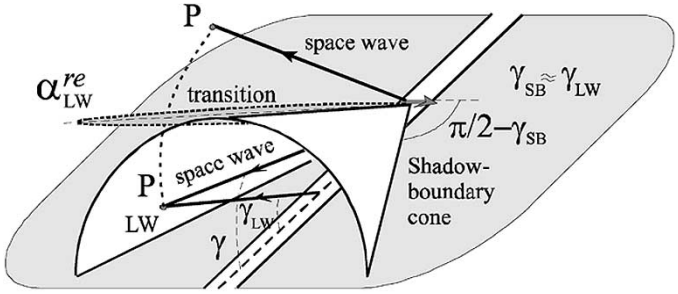

Fig. 6. Shadow boundary cone and compensation mechanism at shadow boundary. The transition region is a conical region with cone angle $\alpha_{\rm LW}^{\rm re}$ and elliptical cross-section (see geometrical details of the ellipse in Fig. 7). The shadow boundary cone, which defines the existence region of the leaky wave, has an angle $\gamma_{SB} \approx \gamma_{\rm LW}$, where $\gamma_{\rm LW}$ is the angle of LW ray propagation (compare with Fig. 5 and Table II). The space-wave ray as well as the leaky-wave ray is also reported for observation points inside and outside the shadow boundary cone (compare with Fig. 1).

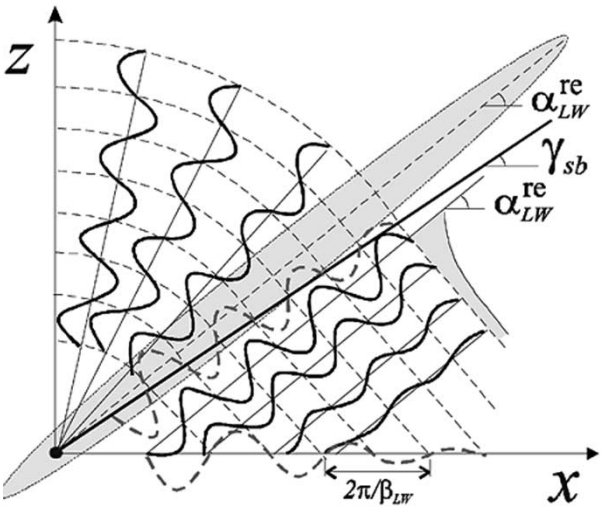

Fig. 7. Graphical representations of leaky wave and space wave. The figure shows matching of spherical space-wave phase-fronts with cylindrical leaky-wave phase-fronts along γ_{SB}. The LW is now observed along directions parallel to $\alpha_{\rm LW}^{\rm re}$, where no attenuation occurs. Increasing x implies lower equi-amplitude oscillations. The ellipse denotes the region were the space wave exhibits a transition in order to compensate for the discontinuity of the leaky wave at the shadow boundary.

(31) becomes asymptotically negligible with respect to the first one. This latter is the same as that derived in (14) with the simple spatial approach; consequently:

$$\tilde{I}_{\rm sdp} \to F^{\rm space} = -\frac{e^{-jk_2 r}}{2\pi r D(k_2 \cos\gamma)} \quad \text{for } \gamma \text{ outside the transition region.} \quad (36)$$

For small argument of the transition function (i.e., inside the transition region) from (32) we see that the dominant contribution is the last one

$$\tilde{I}_{\rm sdp} \to \pm\frac{1}{2} I_{\rm LW} \quad \text{for } \gamma \text{ inside the transition region} \quad (37)$$

where the sign $+(-)$ applies to $\gamma = \gamma_{sb} + \epsilon$ $(\gamma = \gamma_{sb} - \epsilon)$ with ϵ vanishing and positive. Thus, it is clear that the SDP at the shadow boundary compensates for the discontinuity given by the leaky-wave contribution. This compensation occurs at the shadow boundary cone $\gamma = \gamma_{sb}$, where the phase of the LW matches that of the space wave. The graphical representation in Fig. 7 illustrates this mechanism. The phase wavefront of the space wave at distance $\lambda_2/2$ matches at γ_{sb} the phase wavefront of the leaky wave. In contrast with the representation in Fig. 5, the leaky wave oscillations are now observed along lines parallel to the direction of propagation $\alpha_{\rm LW}^{\rm re}$ where they are constant in amplitude; a gradual damping occurs in the orthogonal direction. Since the SB is slanted with respect to the direction of propagation, observing along γ_{sb} the LW is slightly attenuated for increasing r (see Fig. 5) but it maintains the phase matching with the space wave. Inside the transition region the space wave exhibits a transition regime for compensating the discontinuity of the LW at the SB. This transition regime must include not only a change in the spreading factor (from spherical to conical) as typically occurs for propagating-wave compensation (see, i.e., GO disappearance compensated by edge diffraction) but also the inclusion of a small exponential damping.

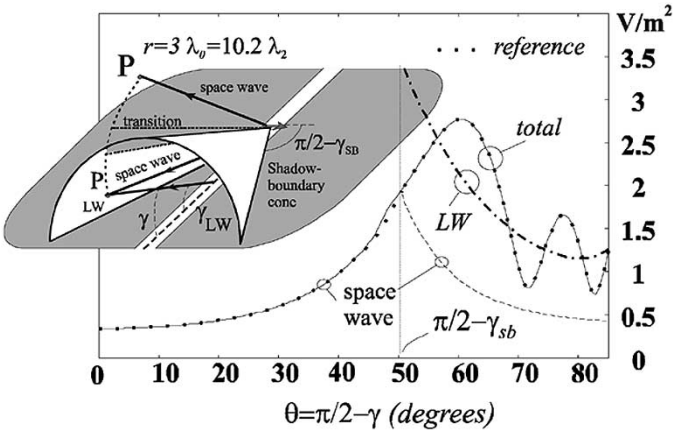

Fig. 8. Electric potential F_2 in medium 2 at a distance $r = 3\lambda_0$ as a function of the scan angle for a slot width $w_s = 3\,10^{-4}\lambda_0$ and for permittivities $\epsilon_{r1} = 1$ and $\epsilon_{r1} = 11.7$. The reference curve (dots) is almost superimposed to the uniform asymptotics (solid line) obtained by implementation of (35). Leaky wave (LW, dash-dotted line) and space wave (dashed line) are also presented.

V. Numerical Examples

Some parametric results are obtained by application of the asymptotic expressions in (35). The example in Fig. 8 checks the accuracy of the asymptotic with respect to a reference solution obtained by numerical space domain integration of (7) (dots). In this figure, the normalized field potential is presented at $r = 3\lambda_0$ versus the scan angle $\theta = 90° - \gamma$, for slots width $w_s = 3\,10^{-4}\lambda_0$ and permittivities $\epsilon_{r1} = 1$ and $\epsilon_{r2} = 11.7$.

The curve relevant to the leaky wave contribution alone is also presented (dash-dotted line), which is truncated at the shadow boundary. The continuity of the total potential across the shadow boundary is guaranteed by the space wave (short dashed line). The sum of the LW and the SW uniformly recovers the reference solution, apart from a minimal deviation before the shadow boundary. This deviations may be attributed to the absence of higher order asymptotic terms.

In the zone where the leaky wave exists one can observe that the total field presents amplitude oscillations due to the interference between leaky and space wave. A maximum of

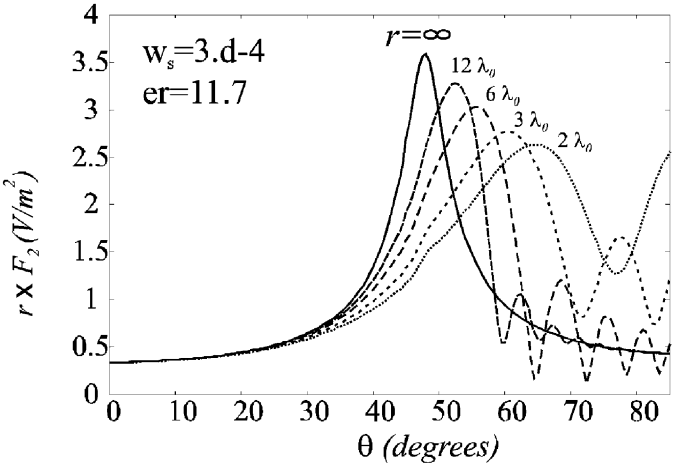

Fig. 9. Normalized electric potential (F_2 multiplied by r) from the near to far zone along radial angular scans at different distances ($r = p\lambda_0, p = 1, 2, 3, 6, 12, \infty$). Slot and permittivities are the same as those in Fig. 3.

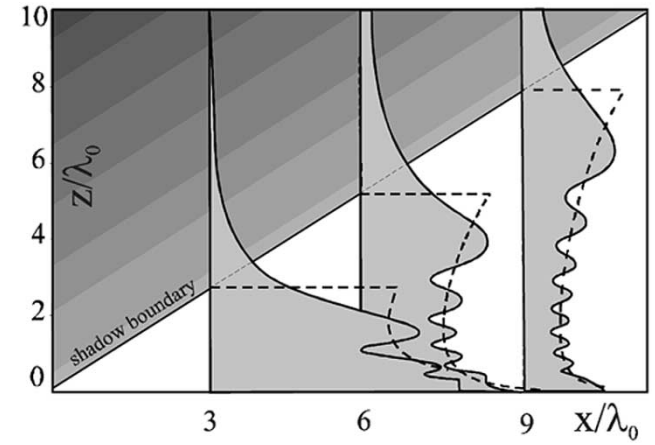

Fig. 10. Vertical scans of the amplitude of the field potential in medium 2 for $y = 0$ and for $x = 3\lambda_0, 6\lambda_0, 9\lambda_0$. Dashed lines represent the exponentially growing (except for points very close to the slot) LW contribution.

the total potential occurs when these two contributions sum in phase beyond the shadow boundary. This maximum gradually approaches the direction of the beam in the far zone. This behavior is presented in Fig. 9. This figure shows an interesting process of reconstruction of the far field lobe previously presented in Fig. 3. For near field scan (e.g., $r = \lambda_0$) the maximum is produced by in-phase interference between leaky and space wave, and it is close to the grazing aspects because of the equalization of the two corresponding ray-path lengths (see Fig. 1). When r is gradually increased, since the leaky wave is exponentially damped along r in its existence region (see Section IV-C), the maximum field is gradually reconstructed by the space wave alone, whose spectrum is modulated in the visible region by the vicinity of the leaky wave pole. Reference solution curves are not presented in Fig. 9 since in all cases superimpose with those relevant to the asymptotic solutions.

Finally, Fig. 10 shows the field potential, calculated via (35), for three vertical scans at $x = 3\lambda_0, 6\lambda_0, 9\lambda_0$ ($\epsilon_{r1} = 1$ and $\epsilon_{r2} = 11.7$, $ws = 3\ 10^{-10}\lambda_0$). The interesting fact is that the intensity grows initially as dominated by the leaky wave. For observation points below the shadow boundary, the amplitude oscillations testify the interference of leaky and space wave, which disappears above the shadow boundary, as expected.

VI. Conclusion

This two part sequence of papers has presented an analytical approximation for the Green's function of an infinite slot printed between two different homogeneous dielectric media. While Part I has dealt with the magnetic current distribution on the slot, this Part II has provided a uniform high-frequency solution which is valid along the entire angular scan and smoothly continuous from near to far zone.

Summarizing the particulars of Part II, we have constructed a ray-optical field structure in the denser medium from a space-domain stationary phase approximation, finding leaky and lateral wave rays emerging from separated points on the slot axis and propagating with the ambient wavespeed along the surface of radiation cones. The aperture of these cones and the position of the diffraction points are intimately related to the wavenumber of the magnetic-currents leaky- and lateral-wave contributions derived in Part I. Together with these rays, space wave-rays phase centered at the source propagate in all directions with spherical spreading factor. Regarding the lateral wave, its higher radial asymptotic order legitimates its negligibility in the subsequent uniform asymptotics.

After this physically appealing ray description, which is discontinuous at a shadow boundary cone of the leaky-wave, a rigorous pole-(saddle-point) uniform asymptotics has been carried out starting from the continuous spectrum representation for the Green's function solution. The relationship between the space-domain nonuniform ray description and the spectral-domain pole-saddle-point treatment has been described with emphasis on the various angular parameters. It has been seen that the limit to the ray regime is reconstructed outside a conical transition volume with elliptical cross section. Inside the same transition volume, the uniform field continuity in an angular scan is demonstrated to be reconstructed by a compensation mechanism between space-wave and leaky-wave discontinuities at the conical shadow boundary.

The gradual description from near to far zone along radial scan is also verified; it is found that the conical leaky-wave is exponentially attenuated along radial scans in its existence region, and therefore disappears in the far zone. The directive pattern is then constructed by the sole space wave contribution, whose directive property is explained by the vicinity of the leaky wave pole to the visible portion of the space-wave spectrum.

The validity and accuracy of the asymptotics has been verified by comparison with independent numerical integration, for observation points up to distance $0.5\lambda_n$, where λ_n $(n = 1, 2)$ is the wavelength pertinent to the medium $n = 1, 2$.

The results obtained, and the physical insight gained, from this prototype solution provide a further building block for extension to more general Green's function problems of open or semi-open waveguiding and leaky structure, whose fundamentals have been treated in the recent literature [2], [5].

REFERENCES

[1] A. Neto and S. Maci, "Green's function of an infinite slot printed between two homogeneous dieletrics. Part I: Magnetic currents," *IEEE Trans. Antennas Propagat.*, vol. 51, pp. 1572–1582, July 2003.

[2] F. Mesa and D. R. Jackson, "The nature of the current excited by a source on a microstrip line," in *Proc. AP-S Symposium and URSI Meeting*, Boston, MA, July 8–13, 2001, p. 266.

[3] C. Di Nallo, F. Mesa, and D. R. Jackson, "Excitation of leaky modes on multilayer stripline structure," *IEEE Trans. Microw. Theory Techn.*, vol. 46, pp. 1062–1071, Aug. 1998.

[4] F. Mesa, C. Di Nallo, and D. R. Jackson, "The theory of surface-wave and space-wave leaky-mode excitation on microstrip lines," *IEEE Trans. Microw. Theory Techn.*, vol. 47, pp. 207–215, Feb. 1999.

[5] D. R. Jackson, F. Mesa, M. J. Freire, D. P. Nyquist, and C. Di Nallo, "An excitation theory for bound modes and residual-wave currents on stripline structures," *Radio Sci.*, vol. 35, no. 2, pp. 495–510, Mar.–Apr. 2000.

[6] T. Rozzi and M. Mongiardo, "Open electromagnetic waveguides," in *Inst. Elect. Eng. Electromagn. Wave Series*, 1997, ch. 7 and 8.

[7] F. Villegas, D. R. Jackson, J. T. Williams, and A. A. Oliner, "Leakage fields from planar semi-infinite trasmission lines," *IEEE Trans. Microw. Theory Techn.*, vol. 47, pp. 443–453, Apr. 1999.

[8] L. B. Felsen and N. Marcuvitz, *Radiation and Scattering of Waves*. Englewood Cliffs, NJ: Prentice-Hall, 1973.

[9] B. L. Van der Waerden, "On the method of saddle points," *Appl. Sci. Res.*, vol. B2, pp. 33–45, 1951.

[10] R. G. Kouyoumjian and P. H. Pathak, "A uniform geometrical theory of diffraction for an edge in a perfectly conducting surface," *Proc. IEEE*, vol. 62, pp. 1448–1461, 1974.

[11] H. Bertoni, A. C. Green, and L. B. Felsen, "Shadowing on inhomogeneous plane wave by an edge," *J. Opt. Soc. Amer.*, July 1978.

Stefano Maci (M'92–SM'99–F'04) was born in Rome, Italy. He received the laurea degree (*cum laude*) in electronic engineering from the University of Florence, Italy, in 1987.

From 1990 to 1998, he was with the Department of Electronic Engineering, University of Florence, as an Assistant Professor. Since 1998, he has been an Associate Professor at the University of Siena, Siena, Italy. His research interests include electromagnetic engineering, mainly concerned with high-frequency and numerical methods for antennas and scattering problems. He was a coauthor of an incremental theory of diffraction, for the description of a wide class of electromagnetic scattering phenomena at high frequency, and of a diffraction theory for the high-frequency analysis of large truncated periodic structures. He has been and presently is responsible for several research contracts and projects supported by national and international institutions, like the European Union, the European Space Agency (ESA-ESTEC, Noordvjiik, The Netherlands), and by industry and research centers. In the sixth EU framework program, he is involved in the Antenna Center of Excellence. In 1997, he was an Invited Professor at the Technical University of Denmark, Copenhagen. He has been an Invited Speaker at several international conferences and Ph.D. courses at European universities, industries, and research centers. He is principal author or coauthor of 40 papers in IEEE Journals, 40 papers in other international journals, and more than 150 papers in proceedings of international conferences.

Dr. Maci received the "Barzilai" prize for the best paper at the XI RiNEm (national conference of electromagnetism) in 1996. He was an Associate Editor of IEEE TRANSACTIONS ON ELECTROMAGNETIC COMPATIBILITY and Convenor at the URSI General Assembly. He is presently a member of the Technical Advisory Board of the URSI Commission B and a member of the advisory board of the Italian Ph.D. School of Electromagnetism. He served as Chairman and Organizer of several special sessions at international conferences and has been chairman of two international workshops. He is currently a Guest Editor of the IEEE TRANSACTIONS ON ANTENNAS PROPAGATION's Special Issue on Artificial Magnetic Conductors, Soft Hard Surfaces, and Other Complex Surfaces.

Andrea Neto (M'00) received the laurea degree (*cum laude*) in electronic engineering from the University of Florence, Italy, in 1994 and the Ph.D. degree in electromagnetics from the University of Siena, Italy, in 2000.

His research interest is concerned with analytical and numerical methods applied to antennas and microwave circuits, with emphasis on large printed arrays and dielectric lens antennas. Part of his Ph.D. has been developed at the European Space Agency Research and Technolgy Center, Noordwijk, the Netherlands, where he has been working for the antenna section for over two years. In the years 2000–2001, he has been a Post Doc at California Institute of Technology, Pasadena, working for the Sub-mm Wave Advanced Technology Group of the Jet Propulsion Laboratory, Pasadena. Since 2002, he is a Senior Antenna Scientist at the Radar Technology Group of the Physics and Electronics Laboratory (FEL) of TNO, Den Haag, The Netherlands.